Fault-Tolerant Control Allocation on a Compound Helicopter in Cruise

Praneet Vayalali PhD Student
Michael McKay PhD Student
Farhan Gandhi Redfern Chair, Director
Center for Mobility with Vertical Lift (MOVE)
Rensselaer Polytechnic Institute
Troy, NY United States

ABSTRACT

The present study provides a comparison of an adaptive versus a robust baseline pseudoinverse control allocation method on a 20,110 lb compound helicopter post-actuator failure. Failure scenarios such as locking of the main rotor swashplate actuators and aerosurface actuators are taken into consideration in forward flight. A range of tolerable positions for locked-in-place actuator failures is established for the aircraft at a cruise speed of 150 knots. A full authority model following linear dynamic inversion control architecture is implemented for the nonlinear simulation model. Stability margins, phase delay, bandwidth, and disturbance rejection specifications for the aircraft were evaluated under different actuator failures with adaptive and robust control allocations. Nonlinear simulations are used to examine the benefits and drawbacks of an adaptive and robust control allocation schemes when the aircraft is subjected to different actuator failure at their extreme positions.

NOTATION

$\vec{x}$	State Vector
$\vec{u}$	Control Input Vector
u, v, w	Body Velocities, ft/s
p, q, r	Body Angular Rates, rad/s
ϕ, θ, ψ	Body Roll, Pitch and Yaw Attitude, deg
x, y, z	Inertial Positions, ft
β_0	Rotor Coning, rad
β_{1s}	Lateral Flap, rad
β_{1c}	Longitudinal Flap, rad
β_d	Differential Flapping, rad
$\dot{\beta}_0$	Rotor Coning Derivative, rad/s
$\dot{\beta}_{1s}$	Lateral Flapping Derivative, rad/s
$\dot{\beta}_{1c}$	Longitudinal Flapping Derivative, rad/s
$\dot{\beta}_d$	Differential Flapping Derivative, rad/s
λ_0	Main Rotor Uniform Inflow
λ_{1s}	Main Rotor Lateral Inflow
λ_{1c}	Main Rotor Longitudinal Inflow
$\lambda_{0_{TR}}$	Tail Rotor Uniform Inflow
Ω	Main Rotor Rotational Speed, rad/s
θ_0	Collective Pitch, deg
θ_{1c}	Lateral Cyclic Pitch, deg
θ_{1s}	Longitudinal Cyclic Pitch, deg
θ_{ped}	Tail Rotor Collective Pitch, deg
θ_{prop}	Propulsor Feathering, deg
θ_{flap}	Flap Deflection, deg
θ_{ail}	Aileron Deflection, deg
θ_{rud}	Rudder Deflection, deg
θ_{stab}	Stabilator Pitch Incidence, deg
s_{lat}	Lateral Actuator Position, inches
s_{fwd}	Forward Actuator Position, inches
s_{aft}	Aft Actuator Position, inches
s_{ped}	Pedal Actuator Position, inches
$M_{\theta/S}$	Mechanical Mixer
τ_p	Equivalent Phase Delay, sec
ω_{BW}	Bandwidth Frequency, rad/s
DRP	Disturbance Rejection Peak, dB
ω_{DRB}	Disturbance Rejection Bandwidth Frequency, rad/s

Presented at the Vertical Flight Society's 77th Annual Forum & Technology Display, Virtual, May 10–14, 2021.

INTRODUCTION

Aircraft survivability in the event of component failure or some loss of control effectiveness is an important area of research, particularly with regards to the control system design. For fixed wing aircraft, utilization of control redundancy has been explored for enabling safe flight despite a loss or degradation in control surface performance. This work is contained largely in the Air Force's *Self-Repairing Flight Control System (SRFCS)* program, which resulted in the design and testing of a reconfigurable modified pseudoinverse-type control mixer which was able to maintain trimmed flight despite failure or loss of a control surface (Refs. 1, 2), as well as the *Reconfigurable Control for Tail-less Fighter Aircraft (RESTORE)* program, which highlighted the ability to reconfigure aircraft control laws when a control effector was locked-in-place (Ref. 3).

While there has been considerable work on exploitation of control redundancy for fixed-wing aircraft survivability, corresponding work in rotary-wing aircraft has been relatively limited. Hess (Ref. 4) attributes this to the lack of redundant control effectors on conventional rotorcraft. In the same work the author presents a pseudo-sliding mode control system for the UH-60A in hover, demonstrating robustness to variation in actuators, control system, vehicle characteristics,

and sensors (also showing a degradation in the vehicle handling qualities). Other rotorcraft focused studies include those by Heiges (Ref. 5), where proven fixed-wing reconfiguration strategies were shown to be effective if sufficient redundancy exists in the system, as well as Enns and Si (Ref. 6), which focused on a reconfigurable swashplate control for fault tolerance.

Recently, work at RPI has explored control reconfiguration to compensate for swashplate actuator failures in trim on compound helicopters (Ref. 7) and on a lift-offset coaxial-pusher helicopter (Ref. 8). Vayalali et al. (Ref. 9) continued this work, examining the effectiveness of the horizontal stabilator on a UH-60 Black Hawk to compensate for certain swashplate actuator locked-in-place failures, concluding that introducing the stabilator as a control input in the feedback loop for the control system post-failure allows the system to re-trim in flight simulation. The same group (Ref. 10) then included redundant controls in the feedback control laws for the aircraft at all times, alleviating the need for control reconfiguration post-failure, and evaluated aircraft handling qualities for such a control architecture.

Typical legacy rotorcraft utilize a control ganging method where the controls are ganged into four groups corresponding to the four control axes. This approach was used in Refs. 9-10 to allocate the longitudinal authority between the main rotor swashplate and the stabilator. When multiple redundant effectors are present, as in the case of a high-speed compound helicopter or other advanced configuration, these effectors can be utilized to the fullest extent based on different objectives via allocation methods (Refs. 11–14).

Previously, the authors (Ref. 15) examined the use of an adaptive pseudoinverse control allocation and its effectiveness for different types of actuator failure on a high-speed compound helicopter platform. The goal of the present work is to explore the possibility of a *robust* pseudoinverse control allocation that would make the aircraft system tolerant to actuator failures and obviate the need for online fault detection and identification. The study will also examine the robustness of the overall system through flight simulation and handling qualities based analysis on a high-speed compound helicopter platform.

APPROACH

Modeling

The compound helicopter configuration used in this study is based on a modified version of the UH-60A Black Hawk simulation model developed by Krishnamurthi and Gandhi (Ref. 16), which is a derivative of Sikorsky's GenHel model (Ref. 17). Validation of this simulation model was performed in Ref. 16 against a trim sweep and frequency responses of flight test and GenHel data from Ref. 18, for a gross weight of 16,000 lbs and altitude of 5,250 ft. The model includes a non-linear, blade element representation of a single main rotor with articulated blades using airfoil table lookup. The blades themselves are approximated to be rigid, undergoing rotations about offset hinges. The 3-state Pitt-Peters dynamic inflow model (Ref. 19) is used to represent the induced velocity distribution on the rotor disk, while the tail rotor thrust and torque are based on the closed-form Bailey rotor (Ref. 20) with a Pitt-Peters 1-state dynamic inflow model. The rigid fuselage and empennage (horizontal and vertical tail) forces and moments are implemented as look-up tables based on wind tunnel data from the GenHel model (Ref. 17).

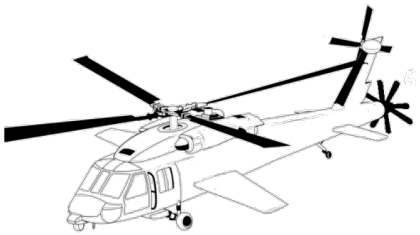

Figure 1. Compound Helicopter Schematic

The aircraft in the proposed study is a lift and thrust compounded derivative of the aforementioned UH-60A Black Hawk model so as to operate at high speeds (up to 250 knots). A fixed wing (with ailerons) and a coaxial propulsor, which is used to provide auxiliary thrust in high-speed flight, are added to the baseline helicopter (Fig. 1). Since the auxiliary thrust is provided by the propulsor, the forward shaft tilt present in the UH-60A is removed. Additionally, the Black Hawk's nonlinear blade twist is replaced by a -8° linear twist. Lowering the twist improves the aerodynamics in high-speed forward flight by reducing the negative lift and large drag on the advancing blade tips Ref. 21. The forces and moments of the wing are found by using Prandtl's lifting line theory, as described in Ref. 22. Interference effects between the wing and rotor are not modeled in this study as it was shown that these effects if included were shown to increase the total power by less than 1% (Ref. 23). The propulsor thrust, torque, and power is modeled using a modified version of Goldstein's vortex theory, combined with blade element theory (Refs. 22 and 24). The aircraft gross weight is increased to 20,110 lbs based on the gross weight of the Piasecki X-49A Speed Hawk, which provides a reasonable approximation for the total weight of a compound aircraft with the addition of the wing, auxiliary propulsion, additional structural weight, and any other changes that must be made. Key properties of the aircraft used in the simulation are provided in Table 1 taken from Ref. 21.

The governing equations of motion are given by

$$\begin{aligned} \dot{\vec{x}} &= f(\vec{x},\vec{u}) \\ \vec{y} &= g(\vec{x},\vec{u}) \end{aligned} \tag{1}$$

where $\vec{y}$ is a generic output vector. The state vector $\vec{x}$, is given by

$$\vec{x} = [\vec{x}_{fuselage},\ \vec{x}_{rotor},\ \vec{x}_{tailrotor}] \tag{2}$$

The state vector comprises of :

$$\begin{aligned} \vec{x}_{fuselage} &= [u,v,w,p,q,r,\phi,\theta,\psi,x,y,z] \\ \vec{x}_{rotor} &= [\beta_0,\beta_{1s},\beta_{1c},\beta_d,\dot{\beta}_0,\dot{\beta}_{1s},\dot{\beta}_{1c},\dot{\beta}_d,\lambda_0,\lambda_{1s},\lambda_{1c}] \\ \vec{x}_{tailrotor} &= [\lambda_{0_{TR}}] \end{aligned} \tag{3}$$

Table 1. Compound Helicopter Configuration Details

Parameter	Value
Gross Weight	20,110 lbs
C.G. Location	1.5 ft aft, 5.8 ft below hub
Main Rotor	
Rotor Radius	26.8 ft
Nominal Rotor Speed	258 RPM
Nominal Blade Twist	-8°
Shaft Tilt	0°
Blade Airfoils	SC-1094 R8/SC-1095
Stabilator	
Effective Area	43 ft^2
Airfoil	NACA 0012
C.P. Location	29.9 ft aft, 5.9 ft below hub
Wing	
Effective Area	226 ft^2
Mean Chord	5 ft
Aspect Ratio	9.0
Taper Ratio	0.825
Incidence Angle	1.25°
C.P. Location	0.5 ft aft, 6.5 ft below hub
Auxiliary Propulsor	
Radius	4.5 ft
Speed	1,934 RPM
Solidity	0.12
Number of Blades	4 × 2
Efficiency (150 - 250 kts)	0.80-0.87
Location	32.6 ft aft, 5.8 ft below hub

The control input vector for the aircraft model is given by

$$\vec{u} = [\theta_{1c}, \theta_{1s}, \theta_0, \theta_{tr}, \theta_{prop}, \theta_{flap}, \theta_{ail}, \theta_{rud}, \theta_{stab}]^T \quad (4)$$

Actuator Geometry

Collective, lateral and longitudinal cyclic blade pitch $(\theta_0, \theta_{1c}, \theta_{1s})$ are achieved by moving the base of the pitch link from the reference plane of the level swashplate. The non-rotating swashplate orientation is fully defined by the height of the swashplate servo actuators $(s_{lat}, s_{fwd}, s_{aft})$ which actuate to transmit pilot control, as shown in Fig. 2. The servo actuators positions are related to the blade pitch controls $(\theta_0, \theta_{1c}, \theta_{1s})$ by Eqs. 5-10 where k_1 = 11.34 and k_2 = 7. These proportionalities demonstrate that the independent control of θ_0, θ_{1c}, and θ_{1s} is attainable with full control of s_{lat}, s_{fwd}, and s_{aft}.

$$\theta_{1c} = \frac{k_1(s_{fwd}+s_{aft})}{2} - k_1 s_{lat} \quad (5)$$

$$\theta_{1s} = k_1 \frac{(s_{fwd}-s_{aft})}{2} \quad (6)$$

$$\theta_0 = k_2 \frac{(s_{fwd}+s_{aft})}{2} \quad (7)$$

$$s_{lat} = \frac{k_1\theta_0 - k_2\theta_{1c}}{k_1 k_2} \quad (8)$$

$$s_{fwd} = \frac{k_1\theta_0 + k_2\theta_{1s}}{k_1 k_2} \quad (9)$$

$$s_{aft} = \frac{k_1\theta_0 - k_2\theta_{1s}}{k_1 k_2} \quad (10)$$

To produce an increase in collective pitch (θ_0) without changing the cyclic pitches, all three actuators need to be raised the same amount. Isolated increases in longitudinal cyclic pitch (θ_{1s}) result from a differential between the forward and aft actuators, while isolated lateral cyclic pitch (θ_{1c}) variation is accomplished by changing the lateral actuator position.

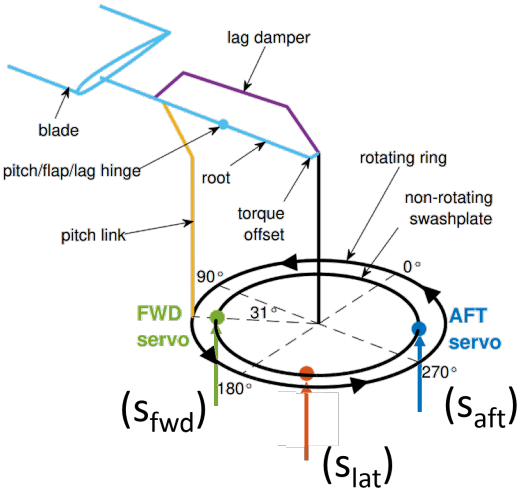

Figure 2. Swashplate Servo Actuator Geometry

The servo naming convention is given relative to the primary effect that each actuator has on the flapping of the rotor (Fig. 2). Increases in the forward actuator height will increase longitudinal cyclic pitch and the rotor will tilt back, increases in the lateral actuator height will decrease lateral cyclic pitch and blade will tilt left side up, and increases in the aft actuator height will reduce longitudinal cyclic pitch and the rotor will tilt forward.

Servo Actuator Failure

The type of actuator failure addressed in the present study is referred to as a *locked condition*, where the input signal to a control actuator yields no response, as the actuator position is locked in place. This type of actuator failure at the swashplate level results in a loss of independent control of the three blade pitches $(\theta_0, \theta_{1c}, \theta_{1s})$ as seen in Eqs. 5-10. Independent control of one is possible (over a certain range), but the two remaining blade pitches are governed by a constraint equation. For example, in the case of s_{fwd} or s_{aft} locked in place, lateral cyclic pitch (θ_{1c}) remains independently controllable (by use of s_{lat}), while longitudinal cyclic (θ_{1s}) and collective pitch (θ_0) become coupled. However, this can be mitigated by offloading the swashplate through the inclusion of the redundant control effectors in the feedback loop throughout operation. In the present study, the redundant control effectors $(\theta_{prop}, \theta_{flap}, \theta_{ail}, \theta_{stab})$ are allocated along with rotor collective and cyclic pitches $(\theta_0, \theta_{1c}, \theta_{1s})$ for all of the relevant control axes, using the pseudoinverse control allocation method (described in a later section).

Control System Design

The control system for the simulation model is designed based on model following linear dynamic inversion (DI) (Ref. 25). Model-following concepts are widely used in modern rotorcraft control systems for their ability to independently set performance and disturbance rejection characteristics. The DI

controller schedules the model with flight condition to eliminate the need for feedback gain scheduling due to similar error dynamics over different flight regimes, making the controller applicable to a wide range of flight conditions (Refs. 25, 26).

In the inner loop, the response type to pilot input is designed for Attitude Command, Attitude Hold in the roll and pitch axes, where pilot input commands a change in roll and pitch attitudes ($\Delta\phi_{cmd}$ and $\Delta\theta_{cmd}$) and returns to the trim values when input is zero. The heave axis response type is designed for Rate Command, Height Hold, where pilot input commands a change in rate-of-climb and holds current altitude when the commanded rate-of-climb is zero. The yaw axis response type is designed for Rate Command Direction Hold, where pilot input commands a change in yaw rate and holds current heading when the yaw rate command is zero. The response type for the outer loop is Translational Rate Command, where pilot inputs command a change in ground speed. With the implementation of the outer loop, the pilot input does not directly command $\Delta\phi_{cmd}$ *and* $\Delta\theta_{cmd}$ as in the inner loop. Rather, they are indirectly commanded by the outer loop through the desired ground speeds. The full 24-state linear model is reduced to an 8-state quasi-steady model for control law design, with state vector is given by

$$\vec{x}_r = [u, v, w, p, q, r, \phi, \theta]^T \tag{11}$$

Pseudoinverse Control Allocation

The pseudoinverse control allocation method is used in the present study because it is significantly more robust than control ganging while computationally less expensive in comparison to a non-deterministic method such as quadratic programming (Ref. 14). The pseudoinverse provides a linear solution for the desired accelerations while minimizing the L_2 norm of the control input vector, u_{cmd}. This type of allocation is typically used for an over-actuated system such as a compound helicopter with redundant actuators. A detailed description of the pseudoinverse control allocation is available in Refs. 12–14. Usually in a dynamic inversion control system, the matrix CB is square and invertible but for the case of overactuated systems, where CB is not square but is full row rank (meaning the matrix has more columns than rows, as in the case of redundant actuators), a pseudoinverse can be applied. The form of the pseudoinverse is as follows:

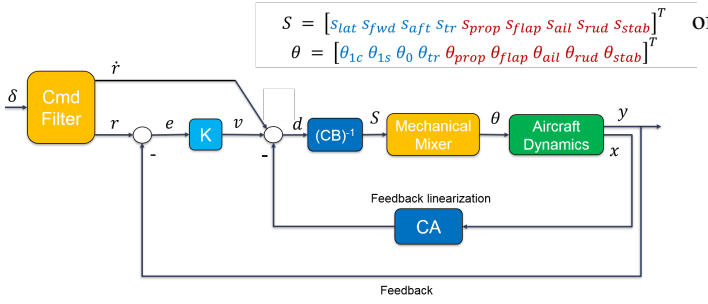

Figure 3. Dynamic Inversion Control Architecture

$$u_{cmd} = (CB)^T((CB)(CB)^T)^{-1}d \tag{12}$$

where u_{cmd} is the control command vector to the actuators, and d is the desired acceleration vector. The control sensitivity matrix, B (which is calculated from an off-line trim routine), relates the control inputs (Eq. 4) to the accelerations. In the present study, the pseudoinverse method maps the accelerations to the actuators rather than the control inputs (Eq. 4) so that actuator failure can be accounted for directly in the allocation. Instead of using the control sensitivity matrix (B) a control actuator sensitivity matrix ($\hat{B}$), is defined as shown in Eq. 13.

$$\hat{B} = BM_{\theta/S} \tag{13}$$

Using Eq. 13 in Eq. 12 gives:

$$S_{cmd} = (C\hat{B})^T((C\hat{B})(C\hat{B})^T)^{-1}d \tag{14}$$

where $S_{cmd} = [s_{lat}, s_{fwd}, s_{aft}, s_{ped}, s_{prop}, s_{ail}, s_{rud}, s_{stab}]^T$, and $M_{\theta/S}$ is the mechanical mixer which represents the mechanical rigging between the actuators (S) and the control effectors ($\vec{u}$). It is important to note that for the outer loop DI controller, the forward speed is mapped to both the pitch attitude and propulsor (because the coaxial propulsor has sensitivity with only the forward acceleration in the body axis). For the baseline compound helicopter, the pseudoinverse control allocation method provides a solution to Eq. 14 such that the actuator input vector (S_{cmd}) has a minimal L_2 norm. In previous work published by the authors (Ref. 15), the control allocation was adapted (recalculation of the pseudoinverse) based on the fault that had occurred in the control actuators. In the present study, no adaptation occurs in the allocation; in the event of an actuator failure, the allocation remains identical to the baseline case and the control effort of the working set of actuators generally must increase to maintain the flight condition.

RESULTS AND DISCUSSION

At a cruise speed of 150 knots, the notional (nose-level) trim of the compound helicopter is given in Table 2.

Table 2. Nominal Trim at 150 Knots

Parameter	Value
Lateral Cyclic Pitch, θ_{1c}	-0.3°
Longitudinal Cyclic Pitch, θ_{1s}	-0.8°
Collective Pitch, θ_0	7.8°
Tail Rotor Collective Pitch, θ_{tr}	8.3°
Propulsor Collective Pitch, θ_{prop}	24° (2,564 lb_f)
Flaps, θ_{flap}	0°
Ailerons, θ_{ail}	0°
Rudder, θ_{rud}	0°
Stabilator, θ_{stab}	4.1°
Roll Attitude, ϕ	2.5°
Rotor Lift Share	62%
Wing Lift Share	30%

Table 3 shows the range of allowable actuator failures at a cruise speed of 150 knots with careful consideration of minimum blade flapping and main rotor geometric control limits as constraints (Table 4). Here, the failed actuator/control effector setting is varied parametrically and a pseudoinverse trim routine (Ref. 15) is used to solve for the rest of the controls.

Table 3. Range of Allowable Failures at 150 knots

Parameter	Trim position	Min	Max
s_{lat}	0.4 in	-0.5 in	1.5 in
s_{fwd}	0.46 in	-0.14 in	0.8 in
s_{aft}	-1.1 in	-1.6 in	1.2 in
s_{tr}	1.49 in	-1.6 in	1.9 in
$\theta_{left\ ail}$	0°	-25°	30°
$\theta_{right\ ail}$	0°	-30°	25°
θ_{rud}	0°	-1°	7.5°
θ_{stab}	4.1°	-8°	10°

Note that the allowable ranges for the aerosurfaces ($\theta_{left\ ail}$, $\theta_{right\ ail}$, θ_{rud}, & θ_{stab}) are less than the geometric limits (not shown here), which is due to the swashplate geometric limits (main rotor controls) and the minimum blade flapping limits being active in these conditions (Table 4). This implies that the rotor is incapable of compensating the moments generated by the aerosurfaces beyond the established ranges for conditions with sufficient dynamic pressure.

Table 4. UH-60A Main Rotor Control and Flapping Limits (Ref. 17)

Constraint	Limits
Collective Pitch	$0.4^\circ \leq \theta_{75} \leq 16.4^\circ$
Lateral Cyclic Pitch	$-8^\circ \leq \theta_{1c} \leq 8^\circ$
Longitudinal Cyclic Pitch	$-16^\circ \leq \theta_{1s} \leq 16^\circ$
Blade Flapping	$-6^\circ \leq \beta \leq 22^\circ$

Handling Qualities

The gains for the model-following linear dynamic inversion controller (as described in the control system design section) are tuned such that the undamaged baseline aircraft has stable closed loop poles, meets minimum crossover frequency requirements, satisfies stability margin requirements, and enforces the range of integrator-to-proportional gain ratio to be between 10% and 20% of the crossover frequency while minimizing over the crossover frequency (Ref. 27). For this study, failure of the main rotor swashplate actuators, flaperons, and stabilator are taken into consideration.

Figures 4 - 6 represent the pitch axis handling qualities of the baseline undamaged aircraft (blue circle marker) along with failed forward (s_{fwd}), aft (s_{aft}), and stabilator (s_{stab}) actuators represented by the square, diamond and triangle markers, respectively. The green and red colors indicate the minimum and maximum allowable locked-in-place failure cases for each actuator and the hollow and solid markers represent the adaptive and robust pseudoinverse control allocation methods, respectively.

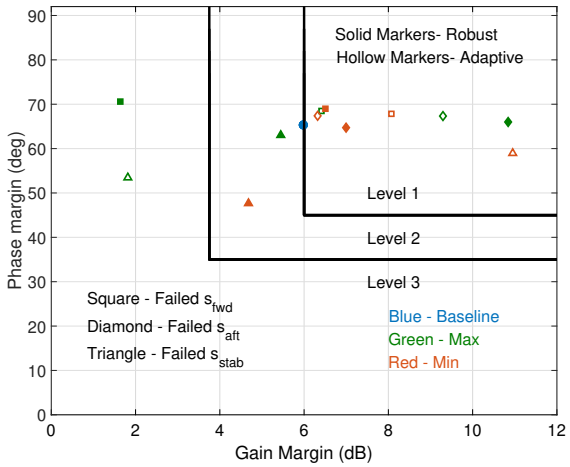

Figure 4. Pitch Stability Margins

Figure 4 shows the pitch axis stability margins (based on Ref. 28). Most of the failed cases, as well as the undamaged baseline aircraft, have Level 1 margins. The exceptions are stabilator failure at the maximum and minimum positions for the robust allocation (solid green and red triangles), which has Level 2 margins, and the failed forward actuator (solid green square) and stabilator (hollow green triangle) at the maximum position for the robust and adaptive allocation, respectively, which fall into Level 3.

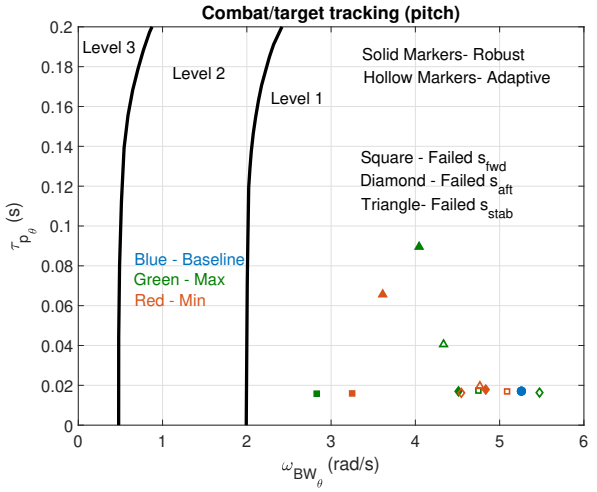

Figure 5. Pitch Phase Delay and Bandwidth

For the same cases, phase delay and bandwidth for pitch axis combat/target tracking and acquisition in forward flight are also generated (Fig. 5) based on (Ref. 29). Post-failure, the redistributed pseudoinverse control allocation (adaptive failed cases) is resolved to make the damaged aircraft response behave similar to the undamaged baseline aircraft (blue marker). This is evident from the clustering of the adaptive failed actuator cases (hollow markers) near the baseline undamaged aircraft. Meanwhile, the same is not true for the robust failed cases where one can note the degradation in the aircraft re-

sponse characteristics particularly for the failed forward actuator (solid green and red square markers) and the failed stabilator (solid green and red triangle markers). Overall, the handling qualities ratings for pitch axis bandwidth and phase delay fall in Level 1 for all cases considered.

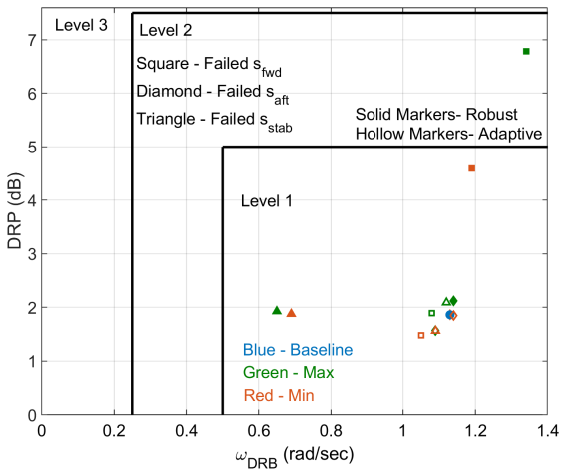

Figure 6. Pitch Disturbance Rejection

Figure 6 represents the pitch axis disturbance rejection metrics at a cruise speed of 150 knots. The majority of the failed cases, as well as the baseline undamaged aircraft, retain Level 1 handling qualities, except for the robust failed forward actuator at the maximum position, which falls to Level 2. Note the clustering of the adaptive failed cases (hollow markers) near the undamaged baseline case. This shows the efficacy of the adaptation post-failure. Meanwhile, the robust allocation shows degradation in the failed stabilator and forward swashplate actuator at extreme positions.

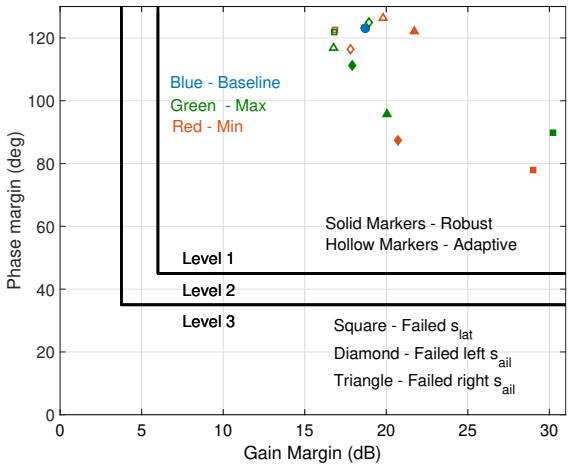

Figure 7. Roll Stability Margins

Figures 7 - 9 represent the roll axis handling qualities of the baseline undamaged aircraft (blue circle marker) along with failed lateral (s_{lat}), left flaperon ($s_{left\ ail}$), and right flaperon ($s_{right\ ail}$) actuators represented by the square, diamond, and triangle markers, respectively, with the green and red colors showing the allowable minimum and maximum locked-in-place failure cases for each actuator.

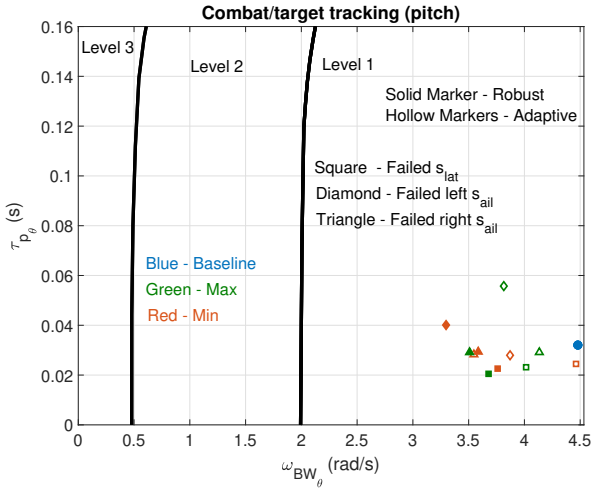

Figure 8. Roll Phase Delay and Bandwidth

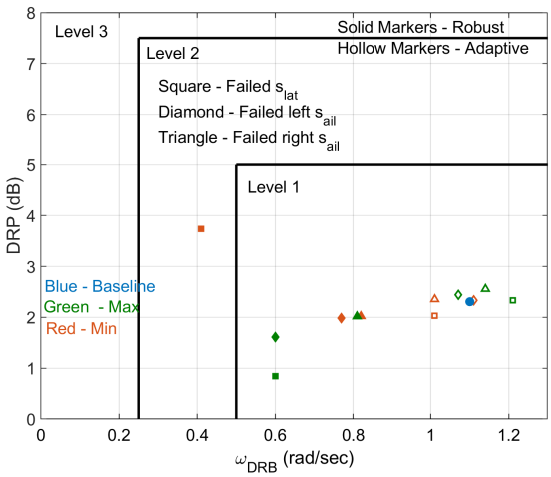

Figure 9. Roll Disturbance Rejection

Overall, figures 7 - 9 show that the aircraft retains Level 1 handling qualities for most of the failed cases (both robust and adaptive allocations), as well as the baseline undamaged case (solid blue marker), with the exception of the robust failed lateral actuator at the minimum position (solid red square) falling to Level 2 in the disturbance rejection metric (Fig. 9). It can be noted that the failed cases with adaptive allocation (hollow markers) cluster near the baseline undamaged case, while there is degradation in the qualities for the failed cases with robust allocation (solid markers).

Now that the handling qualities have been established for the aircraft under different actuator fault scenarios with a comparison of the adaptive and robust control allocation, examining the aircraft response to these faults with the use of robust and

adaptive control allocation is important. The following results are based on the nonlinear simulation of the aircraft, as described in the modeling section, at a cruise speed of 150 knots.

Forward Actuator Failure

Figures 10 - 13 show nonlinear simulations of the minimum allowable position of the failed forward actuator according to the steady-state trim solutions at a cruise speed of 150 knots (Table 3), where the dashed and solid lines represent the robust and adaptive control allocations. Failure in the forward actuator (s_{fwd}) is modeled by moving it by -0.6 inches from nominal trim to its minimum position and locking it in place. Figure 10a shows the time history of the main rotor swashplate lateral, forward, and aft actuator positions from 0 to 90 seconds at 150 knots, with the failure introduced at 10 seconds. From 0 to 10 seconds, the trim positions of the three actuators at 150 knots are shown. At 10 seconds, the forward actuator (s_{fwd}) is moved by -0.6 inches and locked out of trim. In both adaptive and robust cases, the aft and the lateral actuators take up new positions post-failure. Figure 10b shows the longitudinal cyclic (θ_{1s}) on the left axis and the stabilator pitch (θ_{stab}) on the right axis. The decrease in the foward actuator position along with the increase in the aft actuator position results in the longitudinal cyclic (θ_{1s}) becoming more negative, -0.8° to -14° for the adaptive case (solid blue line) and saturates at -16° for the robust case (dashed blue line). This induces a nose-down pitching moment from the main rotor.

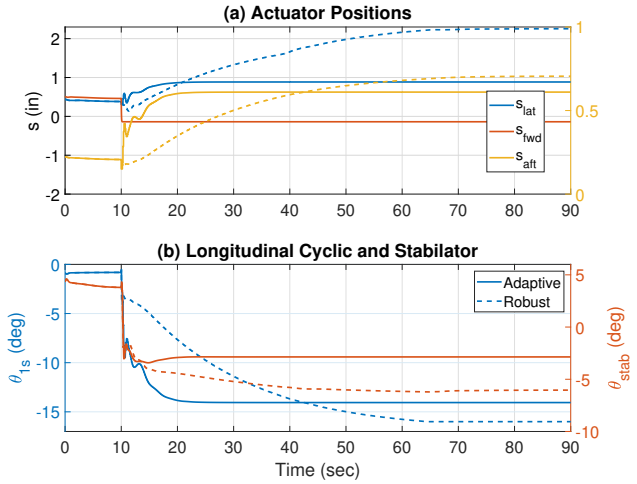

Figure 10. Actuator Positions, Longitudinal Cyclic and Stabilator for Minimum Forward Actuator Failure

At 10 seconds, the adaptive control allocation assumes fault detection has taken place, while the robust baseline allocation does not make use of fault detection. In both cases, the stabilator pitches leading edge down from trim at 4° (solid and dashed red lines) to produce a compensatory nose-up pitching moment. A forward reorientation of the main rotor thrust (relative to the rotor hub) due to the change in the longitudinal

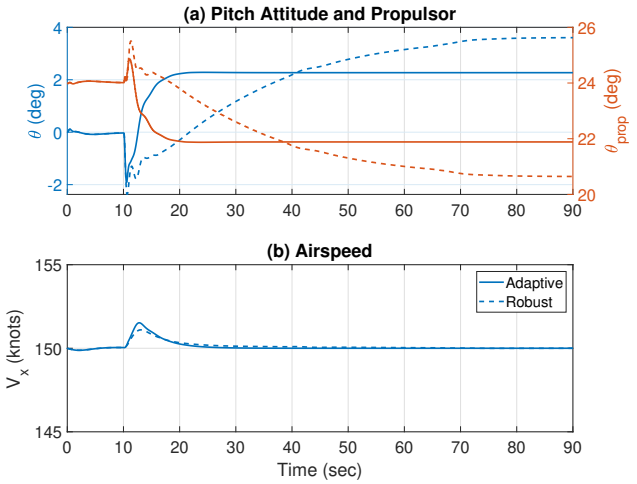

Figure 11. Pitch Attitude, Propulsor Feathering and Forward Speed for Minimum Forward Actuator Failure

cyclic (θ_{1s}), and consequently β_{1c}, also increases the propulsive force from the main rotor. In order to re-balance this propulsive force, the vehicle orients itself to a slightly more nose-up pitch attitude (blue lines in Fig. 11a). In parallel, the propulsor feathering decreases (red lines in Fig. 11a) in order to maintain the commanded airspeed (Fig. 11b).

Figures 12 and 13 show some of the off-axis responses that result from the forward actuator failure. As the lateral actuator increases post-failure (blue lines Fig. 10a) the rotor produces a roll left moment. This results in a more wings-level roll attitude (Fig. 12a) in case of an adaptive allocation (solid line) in comparison to a -10° roll attitude for the robust baseline allocation (dashed line) case, required to maintain a zero sideward velocity (Fig. 12b).

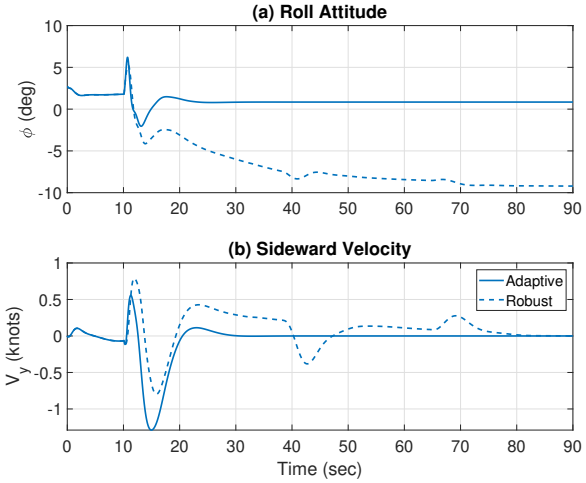

Figure 12. Roll Attitude and Sideward Speed for Minimum Forward Actuator Failure

Figure 13a shows the time history of the main rotor collective (θ_0) on the left axis and wing flaps (θ_{flap}) on the right axis. Post-failure of the forward actuator, the aft actuator increases

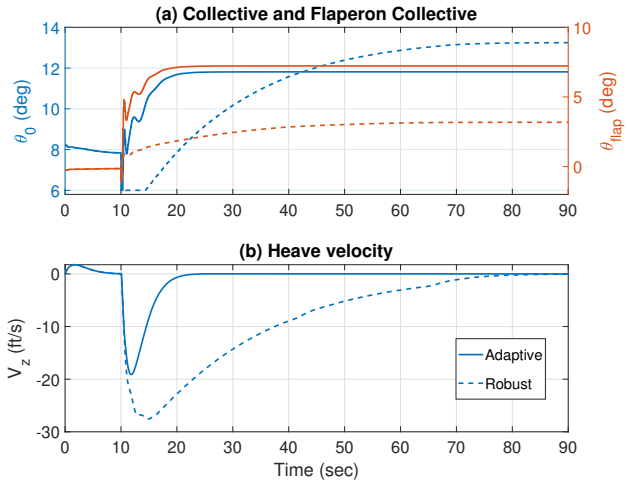

Figure 13. Collective, Flaps and Vertical Speed for Minimum Forward Actuator Failure

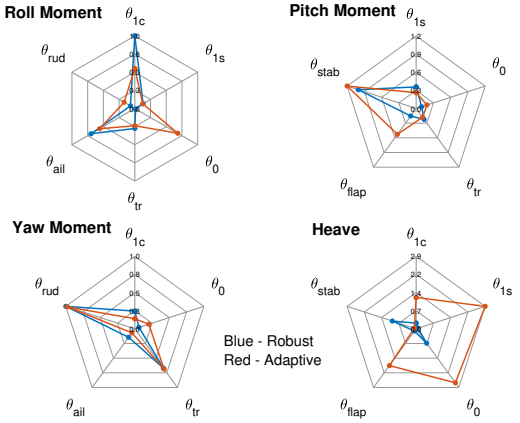

Figure 14. Baseline Robust vs Adaptive Allocation Post-failure of the Swashplate Forward Actuator

to increase the collective in order to maintain zero climb velocity (Fig. 13b). Note that the robust control allocation has a larger time constant and the vehicle achieves zero climb velocity at approximately 80 seconds compared to the faster response in the adaptive case, which returns to zero climb rate at 20 seconds.

Figure 14 shows a comparison of the adaptive and robust baseline control allocations along different axes in case of a forward actuator failure. Examining the roll axis post-failure (red line in roll moment spider plot in Fig. 14), the collective is utilized to achieve roll moments because the adaptive reallocation takes into account the mechanical rigging of the swashplate actuators to the lateral cyclic (Eq. 5 and Eq. 7). This results in the smaller roll attitude change in the case of the adaptive allocation when compared to the robust allocation (Fig. 12a). Along the heave axis, the redistribution by the pseudoinverse leads to a large allocation among the working actuators for the adaptive case (red line in heave spider plot in Fig. 14) in comparison to the baseline robust allocation (blue line). This drastic requirement for allocation is to compensate for the pitch-heave coupling that arises from the forward actuator failure (from Eq. 6 and Eq. 7). Now consider the

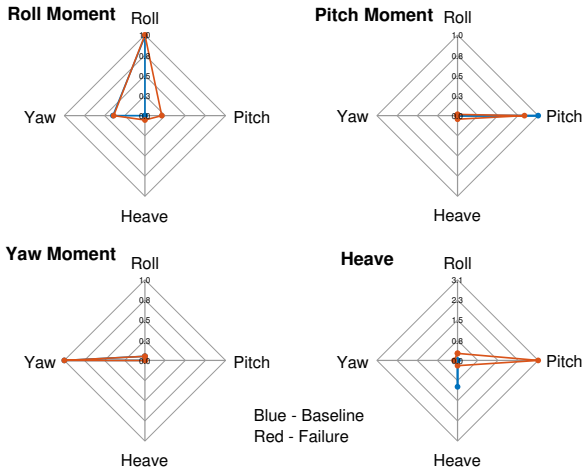

Figure 15. Effect of Robust Control Allocation for Commanded Moments and Thrust for Swashplate Forward Actuator Failure

case of a robust baseline control allocation with no adaption in case of failure. Figure 15 represents the moment and thrust that results from the mixer input. In the baseline aircraft, the pseudoinverse control allocation results in pure control modes (blue line) while in case of failure, the same allocation results in a pitch-heave coupling (red line in heave spider plot) because of the swashplate rigging (Eq. 6 and Eq. 7). Overall, it can be noted that the robust control allocation for forward actuator failure has a degraded response taking a longer time to compensate (over 80 seconds) while the adaptive control allocation is able to recover the aircraft to maintain the desired commands within 10 seconds.

Aft Actuator failure

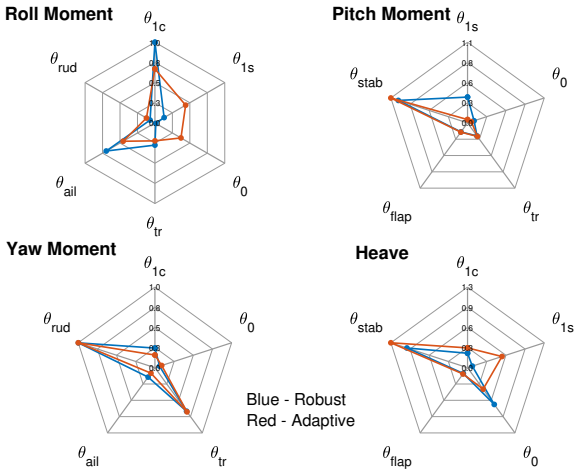

Figure 16. Baseline Robust and Adaptive Allocation Post-failure of the Swashplate Aft Actuator

Figures 16 and 17 show that both the robust and adaptive control allocations are very similar post-failure and with no severe degradation in the desired control modes except for the off-axis roll moment from a commanded heave (red spider plot in Fig. 17).

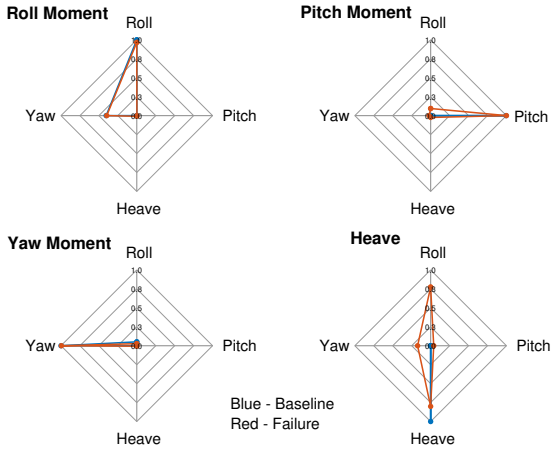

Figure 17. Effect of Robust Control Allocation for Commanded Moments and Thrust for Swashplate Aft Actuator Failure

Failure of the aft actuator at the maximum position is simulated by moving the actuator by 2 inches and locking it in place at 10 seconds (yellow line in Fig. 18a). As a result, both the lateral and forward actuators take up new positions, causing the longitudinal cyclic (θ_{1s}) to become more negative and saturate at -16° in both the adaptive and robust allocation cases (blue lines in Fig. 18b).

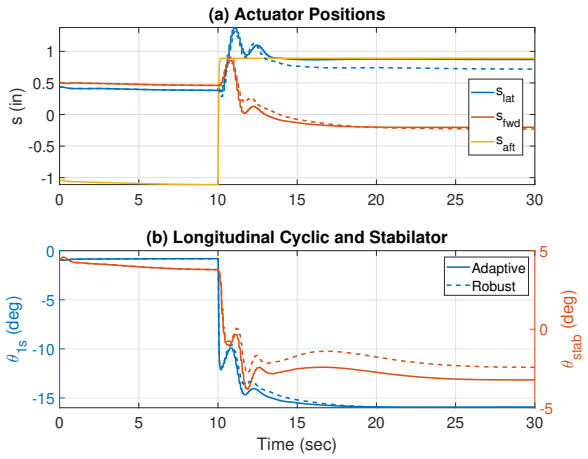

Figure 18. Actuator Positions, Longitudinal Cyclic and Stabilator for Maximum Aft Actuator Failure

A compensatory nose-up pitching moment is produced from the stabilator as it pitches from 4° to near -2.5° for both the cases. The rotor now produces more propulsive thrust because of the reorientation of the main rotor thrust. The aircraft takes up a nose-up pitch attitude and in parallel to this, the propulsor feathering also decreases (Fig. 19a) in order to maintain a forward speed of 150 knots (Fig. 19b). It is important to note that both the adaptive and robust control allocations are able to compensate for failure within 20 seconds which is mainly attributed to the lack of severity in the change of the control modes post-failure. This follows from the aft actuator primarily affecting the retreating side of rotor, which has less negative effects when compared to the forward actuator location that directly affects the advancing side of the rotor (also seen in (Ref. 10)). Although not shown here, similar behavior is observed in when the aft actuator fails at its minimum position for both the adaptive and robust cases. From the two swashplate actuator failures seen so far, the placement of the actuators on the swashplate plays an important role in designing a rotor system that is robust to actuator failure.

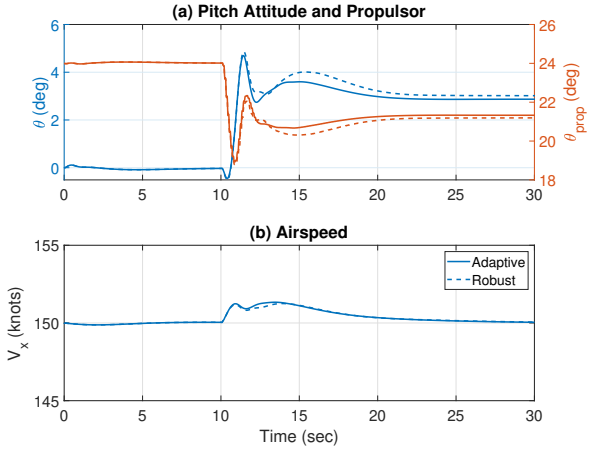

Figure 19. Pitch Attitude, Propulsor Feathering and Forward Speed for Maximum Aft Actuator Failure

Stabilator Failure

Loss of functionality of the aircraft's large stabilator is a possible scenario. Figures 20 - 25 represent the simulations of

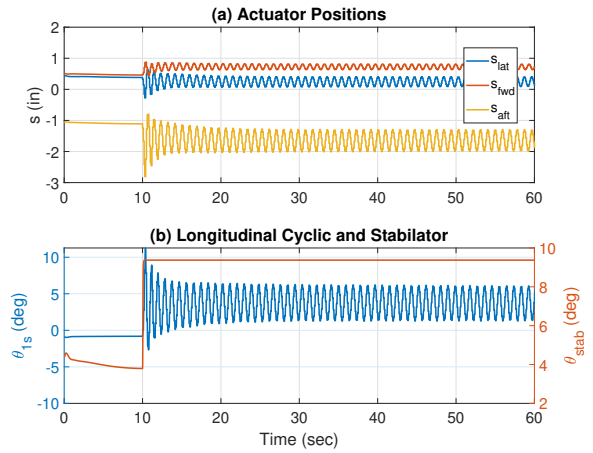

Figure 20. Actuator Positions, Longitudinal Cyclic and Stabilator for Maximum Stabilator Failure with Adaptive Allocation

the adaptive and robust cases for maximum allowable locked stabilator failure according to the steady-state trim solutions (as shown in Table 3). Note that for this case the aircraft has Level 3 and Level 2 stability margins for adaptive and robust cases, respectively. At 10 seconds, failure of the stabilator

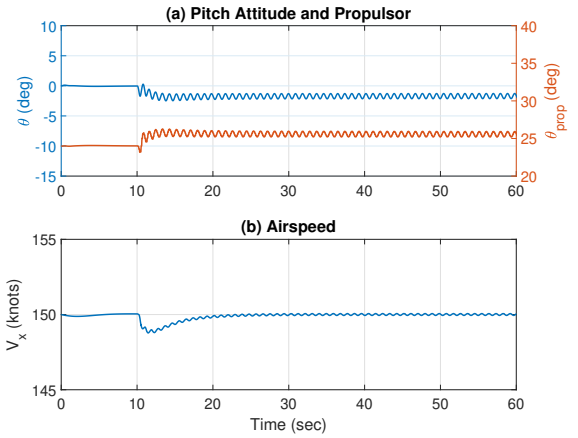

Figure 21. Pitch Attitude, Propulsor Feathering and Forward Speed for Maximum Stabilator Failure with Adaptive Allocation

is simulated by pitching it leading edge up by 6° and locking it in place at its maximum allowable position (red line in Figs. 20b and 23b). In the adaptive case, this locked failure results in a stable response with limit cycle oscillations of the main rotor swashplate actuators (Fig. 20a) while maintaining a cruise speed of 150 knots (Fig. 21b). These stable limit cycles are also observed in the pitch response of the aircraft and is limited to a 1° peak to peak amplitude. Here, the longitudinal cyclic becomes positive meaning the rotor flaps back realigning the aircraft thrust vector. This causes the collective to drop due to the increased upwash from the freestream, leading to saturation at the lower limit of 6° (Fig. 22a), causing the observed limit cycles.

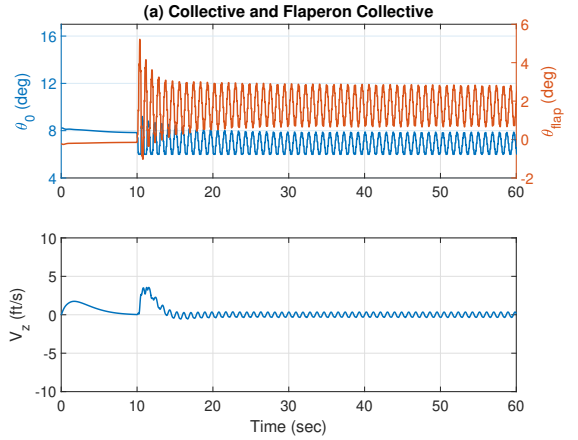

Figure 22. Collective, Flaps and Vertical Speed for Maximum Stabilator Failure with Adaptive Allocation

Meanwhile, it can be noted that for the robust allocation case the collective hits the lower saturation limit during the transients (Fig. 25a) but finally reaches a steady state solution that is away from the saturation, causing the oscillations to die out over a long time period (50 seconds) in the aircraft's response (Figs. 24 and 25b). The collective overall increases in order to compensate for the reorientation of the aircraft thrust vector which in turn is due to the longitudinal cyclic becoming more negative.

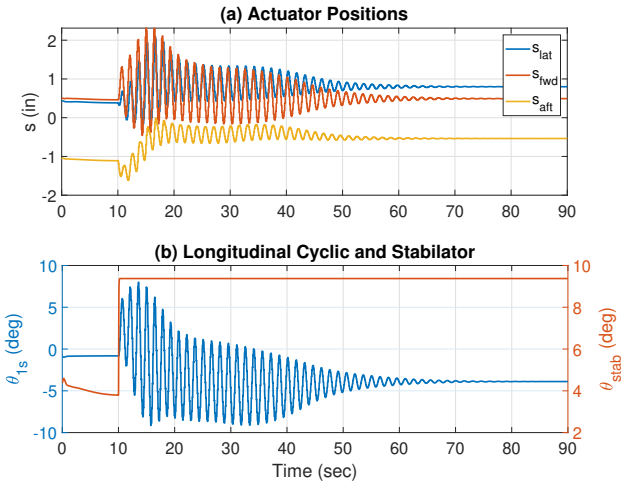

Figure 23. Actuator Positions, Longitudinal Cyclic and Stabilator for Maximum Stabilator Failure with Robust Allocation

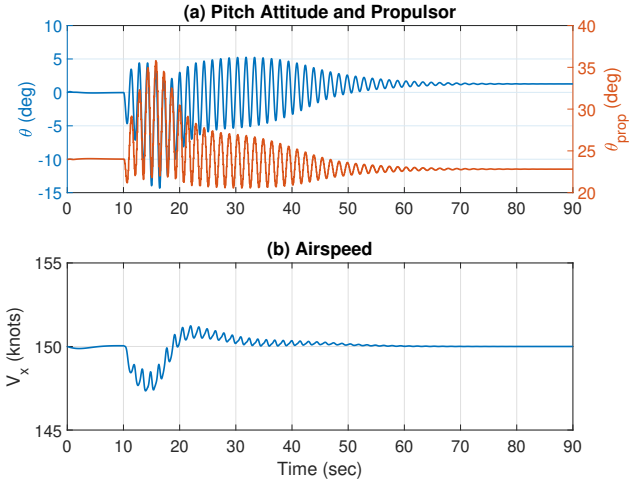

Figure 24. Pitch Attitude, Propulsor Feathering and Forward Speed for Maximum Stabilator Failure with Robust Allocation

It is also important to note that in this case it can be observed that the transient response have a larger amplitude in pitch attitude (Fig. 24a) after the failure in comparison to the adaptive case (Fig. 21a). Overall, both the allocation methods are able to compensate for the stabilator failure.

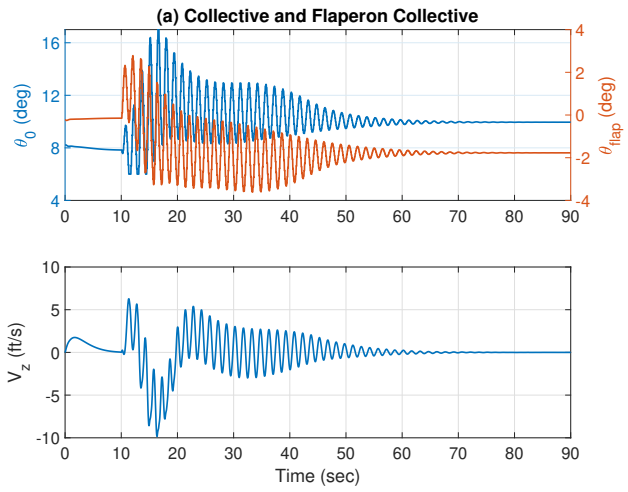

Figure 25. Collective, Flaps and Vertical Speed for Maximum Stabilator Failure with Robust Allocation

Lateral Actuator Failure

Next, use of the ailerons as a redundant effector is examined in the case of lateral actuator failure in the forward flight condition. Figure 26 shows the baseline robust (blue line) and adaptive allocation (red line) for lateral actuator failure. Upon failure, the adaptive allocation reallocates the roll moment authority among the ailerons, longitudinal cyclic, and collective while the control modes along other axes largely remain unchanged. Figure 27 shows the response of the aircraft for commanded moments and thrust for the robust allocation pre and post failure. Here, it can be noted that post-failure of the lateral actuator results in a reduction of roll moment produced from a commanded roll while there is an increase in the off axis pitch and roll moments for a heave command from the aircraft. This is attributed to the swashplate rigging of the actuators (Eq. 5-7).

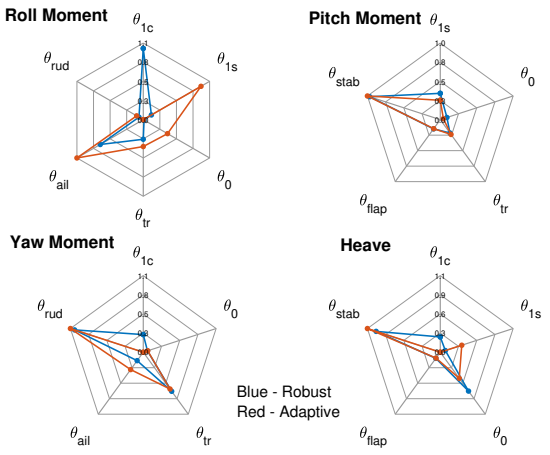

Figure 26. Baseline Robust and Adaptive Allocation Post-failure of the Swashplate Lateral Actuator

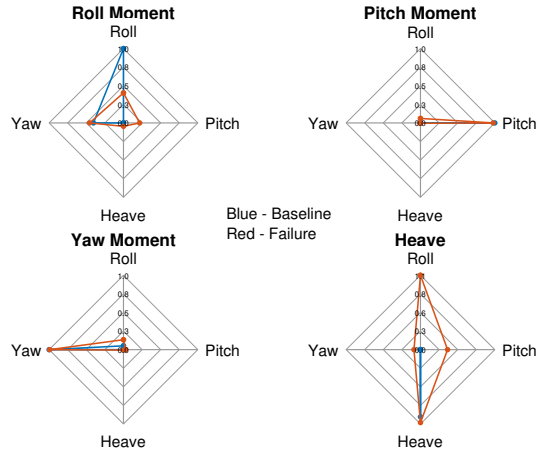

Figure 27. Effect of Robust Control Allocation for Commanded Moments and Thrust for Lateral Actuator Failure

Maximum Lateral Actuator Failure: Failure of the lateral actuator at the maximum position is simulated by moving the actuator position by 1 inch and locking it in place (Fig. 28a) at 10 seconds.

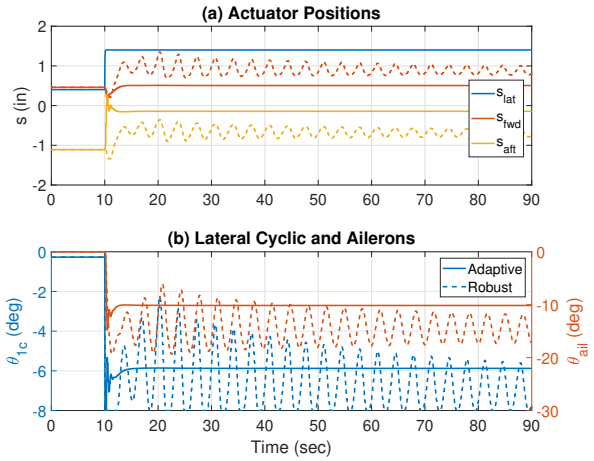

Figure 28. Actuator Positions, Lateral Cyclic, and Ailerons for Maximum Lateral Actuator Failure

Post-failure, only the aft actuator position increases and the swashplate rigging (Eq. 5) causes the lateral cyclic (θ_{1c}) to move from -0.3° to -6° (solid blue line in Fig. 28b) in the adaptive case. Meanwhile, in the robust case both the forward and aft actuator positions increase with a lightly damped oscillatory behavior. This is due to the lateral cyclic saturating at -8°. Overall, the rotor produces a roll right moment because the lateral cyclic decreases, this is compensated by the ailerons which produce a compensatory roll left moment (red lines in Fig. 28b). This causes the aircraft to take up a -10° roll left attitude (Fig. 29a), with the robust case taking up a higher roll attitude (-18°), in order to maintain a zero sideward velocity (Fig. 29b).

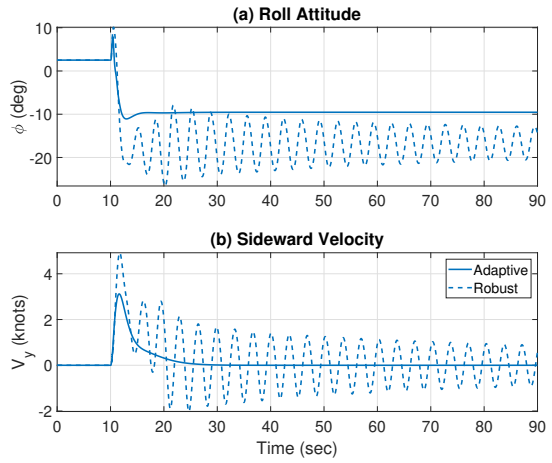

Figure 29. Roll Attitude and Sideward Velocity for Maximum Lateral Actuator Failure

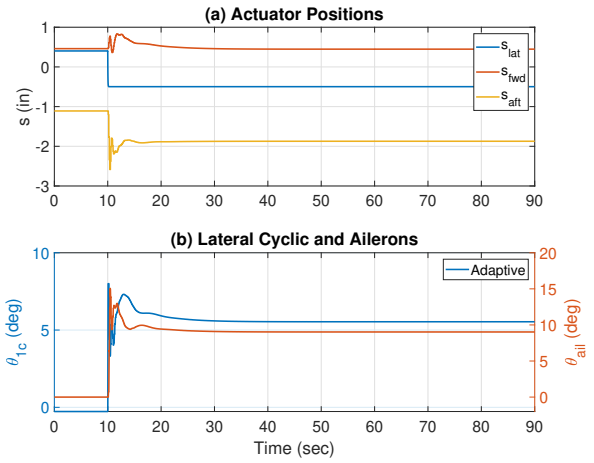

Figure 31. Actuator Positions, Lateral Cyclic, and Ailerons for Minimum Lateral Actuator Failure

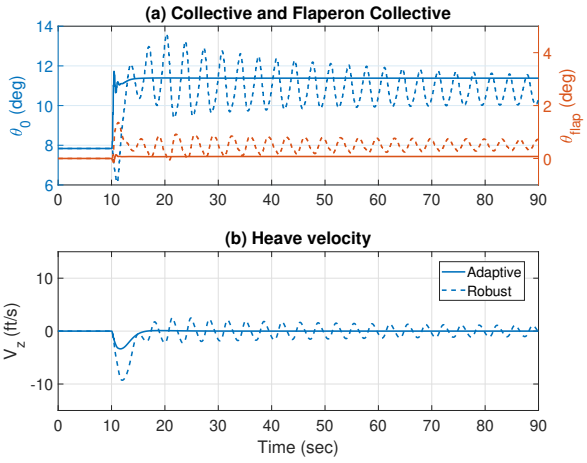

Figure 30. Collective, Flaps, and Heave Velocity for Maximum Lateral Actuator Failure

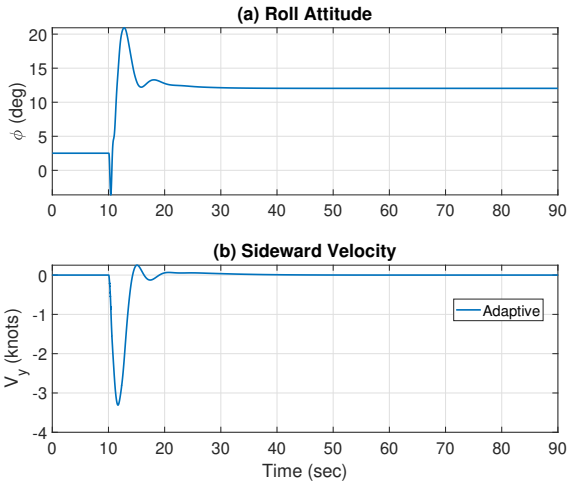

Figure 32. Roll Attitude and Sideward Velocity for Minimum Lateral Actuator Failure

Figure 30a shows the main rotor collective increasing to maintain zero climb velocity (Fig. 30b). Note that in case of the robust allocation the heave transient response is higher in comparison to the adaptive case. Overall, both the allocations work to compensate for failure but the adaptive allocation does not result in saturation and has the aircraft take up a new steady state within 10 seconds of failure with zero oscillatory response.

Minimum Lateral Actuator Failure: In the case of the failure of the lateral actuator at the minimum position it was found that the robust allocation with the outer loop closed did not lead to a stable solution (not shown). Figures 31 - 34 show the simulation of lateral actuator failure for the adaptive allocation. At 10 seconds, the lateral actuator is moved by -0.9 inches (Fig. 31a) and locked. This, along with the decrease in the aft actuator results in an increase of the lateral cyclic (θ_{1c}) (Fig. 31b) producing a roll left moment from the main rotor.

As a consequence, the ailerons pitches differentially to produce a compensatory roll right moment on the aircraft (Fig. 31b). The aircraft takes up a roll right attitude of 12.5° (Fig. 32a) in order to maintain a zero sideward velocity (Fig. 32b). To maintain a zero climb velocity, the main rotor collective (θ_0) and wing flaps (θ_{flap}) decrease (Fig. 33).

During a normal undamaged flight condition, the forward speed (outer loop control allocation) is mapped to both the pitch attitude and the coaxial propulsor. In order to retain overall aircraft stability under minimum lateral actuator failure, the forward velocity is now only allocated to the coaxial propulsor while the inner loop pitch attitude is disengaged from the outer loop, i.e, it is now tracking zero pitch command (blue line Fig. 34a). As a result, the propulsor feathering increases (red line in Fig. 34a) in order to maintain the forward speed of 150 knots (Fig. 34b).

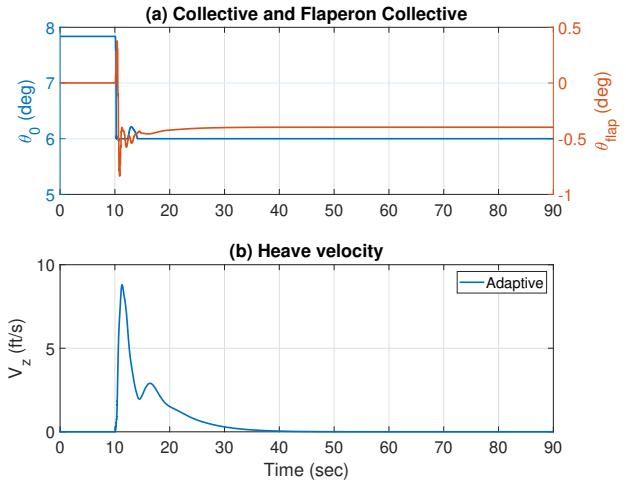

Figure 33. Collective, Flaps, and Heave Velocity for Minimum Lateral Actuator Failure

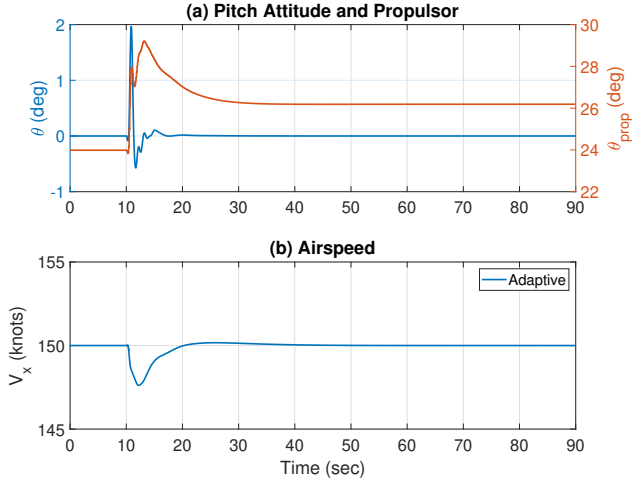

Figure 34. Pitch Attitude, Propulsor, and Forward Velocity for Minimum Lateral Actuator Failure

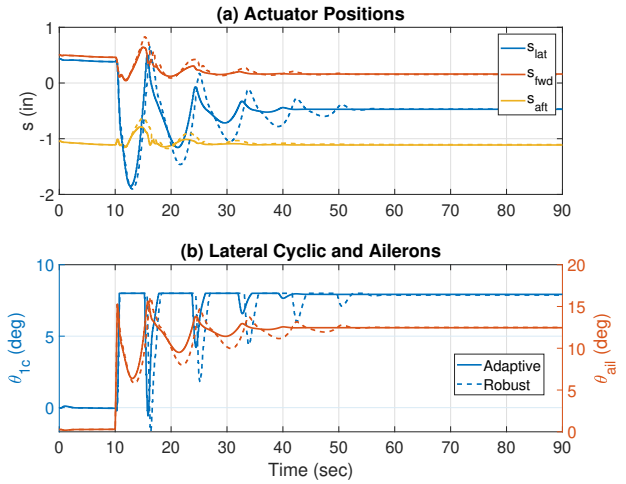

Figure 35. Actuator Positions, Lateral Cyclic, and Ailerons for Maximum Left Flaperon Failure

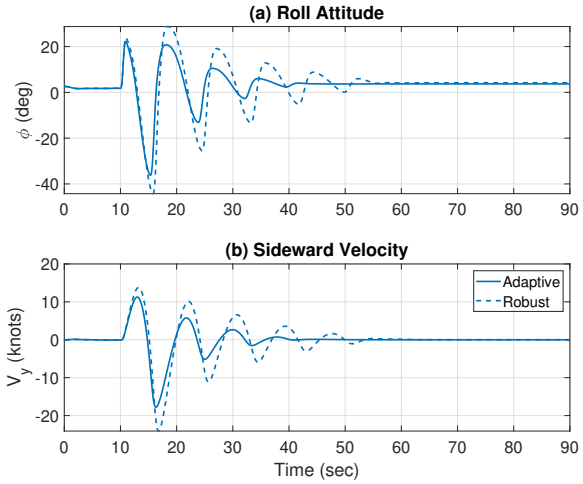

Figure 36. Roll Attitude and Sideward Velocity for Maximum Left Flaperon Failure

Left Flaperon Failure

Another potential point of failure along the lateral axis is the failure of the flaperons. For brevity, only the left flaperon failure is considered here, as failure of the right flaperon will have a mirrored response to the presented case. At 10 seconds, failure of the left flaperon is simulated by moving it by 30° trailing edge down to its maximum allowable position as seen in Table 3. Figure 35b shows the time history of the ailerons, which is a differential input to the flaperons ($\theta_{ail} = \theta_{left\ aileron} - \theta_{right\ aileron}$).

As a consequence of the left flaperon locking out of trim (from 0° to 30°) the wings produce a roll-right moment which is compensated by a roll-left moment from main rotor enabled by the lateral cyclic (θ_{1c}) moving from 0° to saturation at 8° (blue lines in Fig. 35b) which is achieved by moving the lateral actuator (s_{lat}) (Fig. 35a). In addition to this, the right flaperon also moves to produce a compensatory roll-left moment.

Post-failure of the left flaperon, vehicle has a peak transient response of 40° in the roll attitude which finally settles to a slight roll right attitude of 4° (Fig. 36a in order to maintain a zero sideward velocity (Fig. 36b). Upon failure of the left flaperon, the flap control (given by $\theta_{flap} = \theta_{left\ aileron} + \theta_{right\ aileron}$) becomes constrained. So the collective decreases (Fig. 37a) to maintain zero aircraft climb velocity (Fig. 37b). Here, the nonlinear behavior in the transient response of the lateral cyclic is due to saturation. Overall, the aircraft behaves very similarly in both the adaptive and robust control allocations. This is due lack of significant change in the primary aircraft response to commanded thrust and moments in both the control allocation post-failure (not shown here).

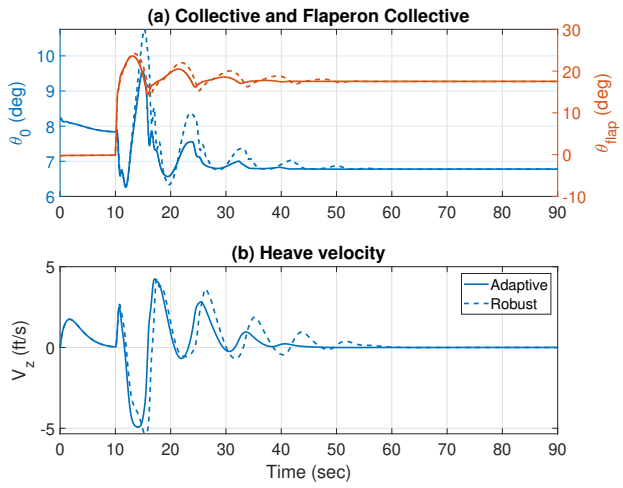

Figure 37. Collective, Flaps, and Heave Velocity for Maximum Left Flaperon Failure

CONCLUSIONS

The present study seeks to compare and contrast the robustness of a baseline pseudoinverse control allocation to an adaptive redistributed pseudoinverse method for different types of actuator failure on a high-speed compound helicopter. Both allocations enable the use of redundant control effectors in both feed-forward and feedback especially to compensate for locked-in-place actuator failures. In the case of an actuator failure, the adaptive method assumes that fault detection has taken place. Meanwhile, the robust method does not make use of any fault information for compensation. The following key conclusions can be drawn from this study:

- A range of allowable failures exist for all actuators from a steady state trim stand point at a cruise speed of 150 knots.
- Stability margins, phase delay, bandwidth, and disturbance rejection specifications for the aircraft were examined using linear models for the baseline and at the failure limit cases with adaptive and robust control allocations.
- The aircraft retains Level 1 in the pitch and roll axes for most cases considered including the baseline undamaged case with some departing Level 1 or even Level 2. Overall, the adaptive method redistributed control authority such that the handling qualities remain close to the undamaged baseline aircraft.
- Nonlinear simulations were conducted to compare and contrast the change in controls and aircraft response post-failure between the robust and the adaptive pseudoinverse methods while also demonstrating their capability.
- For forward actuator failure, the adaptive method substantially reallocates heave control authority because the forward actuator directly affects the advancing side of the rotor leading to significant pitch-heave coupling under failure. Meanwhile, there is no significant change in the control modes of the aircraft when the aft actuator fails. The placement of these actuators on the swashplate plays an important role in designing a rotor system that is robust to failure.
- When the stabilator fails at its maximum allowable position, the adaptive reallocation takes the aircraft to a different steady trim state where the saturation of the collective leads to limit cycle oscillations. Meanwhile, the robust allocation leads to large amplitude lightly damped oscillations.
- For lateral actuator failure, the adaptive method reallocates the roll moment authority while the other control modes largely remain unchanged. For the robust case, the on-axis response degrades along with an increase in the off-axis responses. When failed at the maximum position, the adaptive method has a better response time compared to the saturation effects seen in the robust case. When failed at its minimum position, the robust allocation fails to retain aircraft stability. Meanwhile, for the adaptive method the pitch axis ACAH inner loop is disengaged from the outer loop and forward speed is now only allocated to the propulsor post-failure.
- In the case of left flaperon failure, the aircraft response is similar in both the adaptive and robust cases because of lack of severity in the change of the control modes post-failure.
- Pseudoinverse control allocation is shown to perform well with adaptation because it takes available control sensitivities into account, as well as the mechanical rigging of the main rotor swashplate. For some actuator failures (aft actuator and flaperons), using a robust pseudoinverse allocation (no adaptation) to compensate for failure is a suitable solution. For other actuator failure scenarios, utilizing the baseline robust allocation maintains aircraft stability, which gives sufficient time for the fault to be identified so that the control allocation can adapt and redistribute controls among the working control set, which is shown to improve the vehicle flying qualities.

AUTHOR CONTACT

Praneet Vayalali	vayalp@rpi.edu
Michael McKay	mckaym2@rpi.edu
Farhan Gandhi	fgandhi@rpi.edu

ACKNOWLEDGMENTS

This work is carried out at the Rensselaer Polytechnic Institute under the Army/Navy/NASA Vertical Lift Research Center of Excellence (VLRCOE) Program, grant number W911W61120012, with Dr. Mahendra Bhagwat as Technical Monitor. The authors would also like to acknowledge the

Department of Defense and Army Research Office for sponsoring Mr. McKay through the National Defense Science and Engineering Graduate Fellowship.

REFERENCES

1. Eslinger, R. A. and Chandler, P. R., "Self-Repairing Flight Control System program Overview," *Proceedings of the IEEE 1988 National Aerospace and Electronics Conference*, May 1988, pp. 504–511 vol.2.

2. F. Stewart, J. and L. Shuck, T., "Flight-Testing of the Self-Repairing Flight Control System Using the F-15 Highly Integrated Digital Electronic Control Flight Research Facility," Tech. rep., NASA-TM-101725, 06 1990.

3. Brinker, J. S. and Wise, K. A., "Flight Testing of Reconfigurable Control Law on the X-36 Tailless Aircraft," *Journal of Guidance, Control, and Dynamics*, Vol. 24, No. 5, 2001, pp. 903–909.

4. Hess, R., "A Framework for Robust Rotorcraft Flight Control Design," *Journal of the American Helicopter Society*, Vol. 56, 04 2011, pp. 22004–1.

5. Heiges, M. W., "Reconfigurable Controls for Rotorcraft—A Feasibility Study," *Journal of the American Helicopter Society*, Vol. 42, No. 3, 1997, pp. 254–263.

6. Enns, R. and Si, J., "Helicopter Flight-Control Reconfiguration for Main Rotor Actuator Failures," *Journal of guidance, control, and dynamics*, Vol. 26, No. 4, 2003, pp. 572–584.

7. Reddinger, J. P. and Gandhi, F., "Using Redundant Effectors to Trim a Compound Helicopter with Damaged Main Rotor Controls," *American Helicopter Society 73rd Annual Forum Proceedings*, Fort Worth, TX, May 2017.

8. Mckay, M., Vayalali, P., and Gandhi, F., "Post-Failure Control Reconfiguration on a High-Speed Lift-Offset Coaxial Helicopter," *American Helicopter Society 76th Annual Forum Proceedings*, Virtual, Oct. 2020.

9. Vayalali, P., Mckay, M., Krishnamurthi, J., and Gandhi, F., "Horizontal Stabilator Utilization for Post Swashplate Failure Operation on a UH-60 Black Hawk Helicopter," *Journal of the American Helicopter Society*, Vol. 65, No. 2, April 2020, pp. 1–13(13).

10. Vayalali, P., McKay, M., Krishnamurthi, J., and Gandhi, F., "Fault-Tolerant Control on a UH-60 Black Hawk helicopter using horizontal stabilator," *CEAS Aeronautical Journal*, Oct 2020.

11. Durham, Wayne C, "Constrained control allocation," *Journal of Guidance, control, and Dynamics*, Vol. 16, No. 4, 1993, pp. 717–725.

12. Bodson, Marc, "Evaluation of optimization methods for control allocation," *Journal of Guidance, Control, and Dynamics*, Vol. 25, No. 4, 2002, pp. 703–711.

13. Johansen, T. A. and Fossen, T. I., "Control allocation—a survey," *Automatica*, Vol. 49, No. 5, 2013, pp. 1087–1103.

14. Ivler, C. and Juhasz, O., "Evaluation of Control Allocation Techniques for a Medium Lift Tilt-Rotor," *American Helicopter Society 71rd Annual Forum Proceedings*, Virginia Beach, VA, May 2015.

15. Vayalali, P., Mckay, M., and Gandhi, F., "Redistributed Pseudoinverse Control Allocation for Actuator Failure on a Compound Helicopter," *American Helicopter Society 76th Annual Forum Proceedings*, Virtual, Oct. 2020.

16. Krishnamurthi, J. and Gandhi, F., "Flight Simulation and Control of a Helicopter Undergoing Rotor Span Morphing," *Journal of the American Helicopter Society*, Vol. 63, No. 1, 2018, pp. 1–20.

17. Howlett, J. J., "UH-60A Black Hawk Engineering Simulation Program. Volume 1: Mathematical Model," *NASA CR-166309*, 1981.

18. Ballin, M. G., "Validation of a Real-Time Engineering Simulation of the UH-60A Helicopter," *NASA TM-88360*, 1987.

19. Peters, D. A. and HaQuang, N., "Dynamic Inflow for Practical Applications," *Journal of the American Helicopter Society*, Vol. 33, Oct. 1988, pp. 64–66.

20. Bailey Jr, F., "A Simplified Theoretical Method of Determining the Characteristics of a Lifting Rotor in Forward Flight," *NACA Report 716*, 1941.

21. Reddinger, J.-P. and Gandhi, F., "Physics-Based Trim Optimization of an Articulated Slowed-Rotor Compound Helicopter in High-Speed Flight," *Journal of Aircraft*, Vol. 52, No. 6, 2015, pp. 1756–1766.

22. McCormick, B. W., *Aerodynamics, Aeronautics, and Flight Mechanics*, Wiley, 2nd ed., Sept. 1994, pp. 343–368.

23. Moodie, A. M., and Yeo, H., "Design of a Cruise-Efficient Compound Helicopter," *Journal of the American Helicopter Society*, Vol. 57, No. 3, July 2012, pp. 1–11.

24. Goldstein, S., "On the Vortex Theory of Screw Propellers," *Proceedings of the Royal Society of London. Series A*, Vol. 123, No. 792, Apr. 1929, pp. 440–465.

25. Stevens, B. L., Lewis, F. L., and Johnson, E. N., *Aircraft Control and Simulation: Dynamics, Controls Design, and Autonomous Systems*, John Wiley & Sons, 2015, pp. 477–492.

26. Tischler, M. B. and Remple, R. K., "Aircraft and Rotorcraft System Identification," *AIAA education series*, 2006, pp. 72.

27. Tischler, M. B., Berger, T., Ivler, C. M., Mansur, M. H., Cheung, K. K., and Soong, J. Y., *Practical Methods for Aircraft and Rotorcraft Flight Control Design: An Optimization-Based Approach*, AIAA Education Series, Reston, VA, 2017, pp. 105–170.

28. Anon, "Flight Control Systems—Design, Installation, and Test of Piloted Military Aircraft, General Specification for SAE-AS94900," Tech. rep., SAE International, Warrendale, PA, USA, July 2007.

29. Anon, "Handling Qualities Requirements for Military Rotorcraft," Tech. rep., Aeronautical Design Standard and Performance, Specification ADS-33E-PRF, US Army Aviation and Missile Command, 2000.